Journal of Physics and Chemistry of Solids 114 (2018) 64–70

Contents lists available at ScienceDirect

Journal of Physics and Chemistry of Solids

journal homepage: www.elsevier.com/locate/jpcs

Structural, magnetic and hyperfine characterization of $Zn_xFe_{3-x}O_4$ nanoparticles prepared by sol-gel approach via inorganic precursors

Dzmitry Kotsikau [a,*], Vladimir Pankov [a], Elena Petrova [a], Valentin Natarov [a], Dmitry Filimonov [b], Konstantin Pokholok [b]

[a] Department of Chemistry, Belarusian State University, 220030 Minsk, Belarus
[b] Department of Chemistry, M.V. Lomonosov Moscow State University, 119991 Moscow, Russian Federation

ARTICLE INFO

Keywords:
Magnetic nanoparticles
Structural characterization
Mössbauer spectroscopy
Zn-doped magnetite

ABSTRACT

Structural characteristics and magnetic properties of $Zn_xFe_{3-x}O_4$ (where $x = 0$; 0.09; 0.18; 0.45; 1) nanoparticles were studied with X-ray diffraction (XRD), transmission electron microscopy (TEM), infrared spectroscopy (IR) and vibrating sample magnetometry (VSM). Oxidation of Fe^{2+} ions, redistribution of Zn^{2+} and Fe^{3+} ions between octahedral and tetrahedral sites, and the formation of cation vacancies in spinel-type cubic structure of the obtained $Zn_xFe_{3-x-y}\square_yO_4$ substitutional solid solutions were revealed by ^{57}Fe Mössbauer spectroscopy. The nanoparticles synthesized via a modified sol-gel method using inorganic precursors have a size of 4–10 nm, single-phase composition, superparamagnetic behavior at room temperature (300 K) and a relatively hydrophilic surface to form stable aqueous suspensions. The maximum magnetization of 59 emu/g at 300 K corresponds to $Zn_{0.18}Fe_{2.82}O_4$ composition. The listed features make the materials promising candidates for various biological and medical applications such as contrast-enhanced magnetic resonance imaging, hyperthermia of pathological tissues, controlled drug release, and separation of nucleic acids.

1. Introduction

Nanosized particles based on spinel-type iron oxides, such as magnetite (Fe_3O_4) and maghemite (γ-Fe_2O_3), are promising materials for biomedical applications due to their specific properties and pronounced size effects [1]. In particular, they are widely used in non-invasive radiofrequency-induced hyperthermia of tumors, targeted drug delivery, cell labeling, magnetic separation of biomolecules, and in nuclear magnetic resonance imaging (MRI) as contrasting agents [2–4]. Concerning the biomedical usage, the most important characteristics of magnetic nanoparticles are their grain size and morphology, magnetic properties (namely, specific magnetization and coercivity), surface functionalization, biocompatibility, low toxicity and high stability of colloidal dispersions against aggregation and sedimentation of nanoparticles. Therefore, a development of methods that allow obtaining nanosized materials with the required features is an important task. The main approaches to the preparation of nanoparticles based on iron oxides are chemical co-precipitation from organic and inorganic precursors, microemulsion synthesis, solvothermal method, microwave-assisted synthesis, sonochemical approach, spray pyrolysis, thermal decomposition of organic compounds, etc. [4–8].

However, the magnetic parameters of pure iron oxide nanoparticles are not always optimal for particular biological and medical applications. One of the ways to control the magnetic features of materials consists in their doping with various transition metals (like Zn, Co, Ni) to obtain iron oxide – metal ferrite substitutional solid solutions with spinel-type structure [8–11]. The nature of doping metal, redistribution of metal cations between the sublattices of spinel ferrite structure and their further interactions can have a significant influence on the structural and magnetic properties of the material. The resultant effects depend on the concentration and nature of the dopants, symmetry and ordering degree of the crystal lattice.

Pure magnetite has cubic inverse spinel structure (space group Fd3m) where Fe^{2+} ions and half of Fe^{3+} ions occupy octahedral sites, while the other half of Fe^{3+} ions are in tetrahedral sites. The structure of magnetite can be represented by $(Fe^{3+})[Fe^{2+}Fe^{3+}]O_4$ quasi-chemical formula, where the round and square brackets are assigned to tetrahedral and octahedral positions of the crystalline lattice, respectively. In the past

* Corresponding author.
E-mail address: kotsikau@bsu.by (D. Kotsikau).

https://doi.org/10.1016/j.jpcs.2017.11.004
Received 25 July 2017; Received in revised form 1 November 2017; Accepted 3 November 2017
Available online 4 November 2017

decade, Zn-substituted magnetite nanoparticles have attracted a considerable attention due to versatile wet-chemical preparation methods and high magnetization values. Another advantage of using zinc as a dopant is its relatively low toxicity compared with conventionally used metals like cobalt, nickel and manganese [12]. This makes Zn-substituted magnetite a promising material for biomedical applications.

The properties of the materials mentioned above were found to depend strongly on the concentration and distribution of zinc ions. Generally, the structure of zinc ferrites is represented by $(Zn_y^{2+}Fe_{1-y}^{3+})[Zn_{x-y}^{2+}Fe_{2-x+y}^{3+}]O_4$ quasi-chemical formula, where Zn redistribution between the sublattices depends on the conditions of synthesis. It is known, that well-crystallized zinc ferrite, $(Zn^{2+})[Fe_2^{3+}]O_4$, has a normal spinel structure and exhibits antiferromagnetic behavior with Neel temperature $T_N = 10$ K [13]. In contrast, low substitution of Fe^{3+} ions in tetrahedral sites by diamagnetic Zn^{2+} ions leads to a drop of sub-lattice magnetic moment, which is antiparallel to the Fe^{3+} moment in octahedral sites. An increase in the saturation magnetization of magnetite under slight doping with zinc can be expected as a result of the occurrence of an additional non-compensated magnetic moment. However, the redistribution of zinc and iron ions does not always correspond to the theoretical Zn occupation formula $(Zn_x^{2+}Fe_{1-x}^{3+})[Fe_{1-x}^{2+}Fe_{1+x}^{3+}]O_4$. The use of ^{57}Fe Mössbauer spectroscopy technique presents an important key to study both ions distribution and interactions of sublattices. A detailed description of possible interactions between Zn^{2+}, Fe^{2+} and Fe^{3+} cations in $Zn_xFe_{3-x}O_4$ material is given elsewhere [14,15].

Recently, we have published a study on Zn-substituted nanocrystalline magnetite synthesized via the inorganic modification of sol-gel approach [8]. In this work, we represent an extended study of sol-gel derived Zn-containing ferrites, $Zn_xFe_{3-x-y}\square_yO_4$ with $x = 0$; 0.09; 0.18; 0.45; 1 (where the square stands for cation vacancy). As opposite to the previous work, we have mainly focused here on Mössbauer spectroscopy characterization of the oxidation states of Fe ions and the redistribution of Zn and Fe ions between the octahedral and tetrahedral sites of spinel-type lattice. A wider range of compositions of Zn-containing ferrites has been studied in the present paper. Furthermore, the conditions of synthesis have been revised to provide a better reproducibility of the preparation method.

The applied method of synthesis includes a combined hydrolysis of inorganic metal salts in aqueous solutions under specific conditions to form the corresponding hydroxides or oxides, followed by their subsequent transformation through a series of states: sol, gel, xerogel and a crystalline oxide [16,17]. The use of this approach allows achieving a high homogeneity of the mixed oxides. In addition, the method provides wide possibilities for controlling the functional features of the materials by varying the synthesis conditions, especially the nature of precursors and precipitation agents. Oxide materials obtained via sol-gel method are characterized by a highly hydrated surface, which favors a stabilization of their aqueous dispersions. A certain degree of stability is required for the majority of medical applications of dispersed materials [18,19]. An additional advantage of this approach is its relative technical simplicity and scalability.

The aim of the work was to study the structural characteristics, magnetic properties and hyperfine interactions in $Zn_xFe_{3-x}O_4$ nanosized oxide as a function of zinc content, and to reveal an optimal composition of the solid solution with a maximum increase in the magnetic properties as compared to undoped magnetite.

2. Experimental

2.1. Sample preparation

Sols and nanosized powders of $Zn_xFe_{3-x}O_4$ with x = 0, 0.09, 0.18, 0.45, and 1 have been prepared by sol-gel method using inorganic salts of iron (III), iron (II) and zinc (II) as precursors. The materials were obtained by a slightly modified procedure developed in Ref. [8]. The samples are denoted in the paper as Zn-0, Zn-0.09, Zn-0.18, Zn-0.45, and Zn-1 according to the calculated x values given above. All the chemicals ($Fe(NO_3)_3{\cdot}9H_2O$, $Zn(NO_3)_2{\cdot}6H_2O$ and $FeSO_4{\cdot}7H_2O$) were of analytical grade. The salts were taken in the corresponding ratios. The iron salts molar ratio was constant for all the samples (Fe^{3+}:Fe^{2+} = 2:1). An overall concentration of the salts solution was about 0.1 mole/l. A concentrated solution of NaOH (1 mole/l) taken with a 10% molar excess as compared to the stoichiometric value was used as a precipitation base agent. The reactants were quickly mixed together under vigorous stirring. The synthesis was carried out for 1 h at room temperature (293 K) in nitrogen atmosphere to prevent the oxidation of Fe^{2+} ions by oxygen. The obtained precipitates were washed thoroughly with deionized water by applying magnetic decantation (a NdFeB bar magnet with the field of ~2 kOe was used) to remove all the soluble by-products (nitrate and sulfate ions from the precursors) and the excess of NaOH. To prepare powdered samples of nanoparticles, the aqueous dispersions were dried under vacuum at room temperature. To prepare stable colloidal suspension (sols), the washed dispersion was subjected to ultrasonification with simultaneous addition of diluted NaOH solution until pH of the reaction mixture reached 8. The described conditions of synthesis allowed preparing sols with a narrow size distribution of the nanoparticles, and stable for several days. In contrast to the technique used previously in Ref. [8] (where the sols were stabilized by adding nitric acid), OH^- ions were chosen as particle charge-determining ions. A diluted solution of NaOH was used instead of acid in order to avoid partial dissolution of the oxides, which is possible even in slightly acidic solutions.

2.2. Characterization

The X-ray diffraction (XRD) patterns of powdered samples were recorded in 2θ range of 10–120° on a DRON-2.0 diffractometer using Ni-filtrated Co Kα radiation (λ = 1.78896 Å). An average size of the crystallites (d_{XRD}) was estimated from a broadening of the diffraction reflexes with the Scherrer equation:

$$d_{xrd} = \frac{K{\cdot}\lambda}{[(B-b){\cdot}\cos\theta]} \quad (1)$$

where B is the peak width, b is the instrumental broadening, θ is the Bragg angle, and K is the shape factor ($K \approx 0.89$).

The transmission electron microscopy (TEM) study was carried out on a LEO 906E microscope. Copper grids with a carbon film were dipped into the prepared sols of nanoparticles followed by drying.

The Infrared (IR) spectra were collected from powdered samples in wavenumber range 400–4000 cm^{-1} (resolution is 1 cm^{-1}) on a ThermoNicolet Avatar FTIR-330 spectrometer supplied with a Smart Diffuse Reflectance accessory.

The ^{57}Fe Mössbauer spectra were recorded on a Ms-1104Em (Rostov-na-Donu, Russian Federation) spectrometer using ^{57}Co/Rh source (13.5 mCi) at 78 and 298 K. The fitting procedure was performed with conventional software of minimization of a quadratic functional. All isomer shifts (IS) were referenced to ^{57}Fe in α-Fe at 300 K.

The field-depended magnetization curves were obtained by using a vibration sample magnetometer Cryogen Free Measurement System (CFMS, Cryogenic Ltd. H_{max} = 180 kOe) at both low (5 K) and room (298 K) temperatures. Since the curves did not reach the saturation, the magnetizations measured at 50 kOe were taken as the maximum magnetization values (I_{max}).

3. Results and discussion

The XRD patterns of all the Zn-substituted magnetites given in Fig. 1. are similar to the ones obtained in Ref. [8]. They only contain broad reflections assigned to cubic spinel structure (space group Fd3m), which indicates that single-phased materials are formed. The discussion of the XRD data is given in Ref. [8].

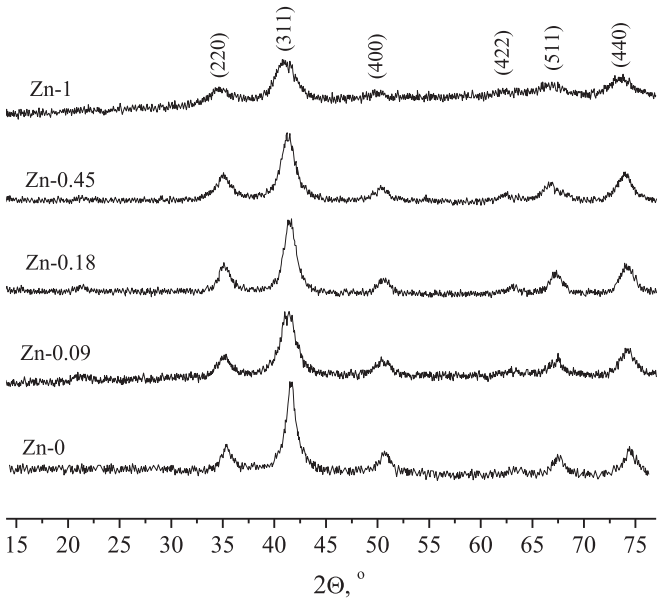

Fig. 1. XRD patterns of $Zn_xFe_{3-x-y}\square_yO_4$ powdered samples.

Table 1
Phase composition, coherently scattering domain size and lattice constants of $Zn_xFe_{3-x-y}\square_yO_4$ ferrites as a function of Zn content according to the XRD data.

Substitution, x	0	0.09	0.18	0.45	1
a, nm	0.8369	0.8385	0.8391	0.8397	0.8425
d_{XRD}, nm	10	10	10	10	8
Phase	spinel	spinel	spinel	spinel	spinel

The structural features of the prepared $Zn_xFe_{3-x}O_4$ materials with x ranging from 0 to 1 are compared together in Table 1.

As seen from Table 1, the values of the lattice parameters rise with increasing Zn content in the $Zn_xFe_{3-x-y}\square_yO_4$ system. The growth of the unit cell parameter is caused by the substitution of Fe^{3+} in tetrahedral coordination of oxygen (0.63 nm) by Zn^{2+} in tetrahedral coordination (0.74 nm), and by the change of Fe^{3+} coordination from tetrahedral (0.63 nm) to octahedral (0.78 nm) [20,21]. Note that the measured lattice parameters, even in case of Fe_3O_4 and $ZnFe_2O_4$ sample where $x = 1$ and $x = 0$, do not exceed the reference data for bulk magnetite (0.839 nm) and stoichiometric zinc ferrite (0.844 nm). This could be an evidence of a partial oxidation of the formed Fe_3O_4 ($a = 0.838$ nm) to γ-Fe_2O_3 with a smaller lattice constant (0.834 nm) [8,22].

Since magnetite is partially oxidized, two possible configurations of the nanoparticles might be formed: i) nanocomposite-like stricture where Fe_3O_4 core is surrounded by γ-Fe_2O_3 shell due to surface oxidation, and/or ii) $Fe_3O_4 - \gamma$-Fe_2O_3 solid solution with a certain concentration of cation vacancies. The composition of the solid solution could be represented via $Fe^{3+}[Fe^{3+}_{1+2\delta}Fe^{2+}_{1-3\delta}\square_\delta]O_4$ quasi-chemical formula, where δ is the concentration of cation vacancies [23].

The spinel-type structure of the samples was additionally confirmed by the IR spectroscopy data given in Fig. 2, which correspond well to the IR-spectra recorded in Ref. [8]. No traces of individual zinc oxide or hydroxides were detected in the IR spectra. Thus, the $Zn_xFe_{3-x}O_4$ solid solutions are obtained within the studied range of zinc concentration. Another evidence supporting this conclusion is a shift of the absorption bands towards lower wavenumbers (548 → 547 → 544 → 539 cm^{-1} for $x = 0.09$, 0.18, 0.45 and 1, respectively). The formation of the solid solutions corresponds with the XRD data described above. The detailed analysis of the IR spectroscopy data is given in Ref. [8].

As mentioned in the experimental section, the colloidal particles prepared here have negative charge due to OH^- ions adsorbed at the solid surface. Whereas in our previous work [8], the particles were charged positively with H^+ ions. IR spectroscopy method is very sensitive to the state of oxide surface. However, the IR spectra recorded from the samples prepared in the present work match closely the spectra reported in Ref. [8]. Therefore, one can conclude that H^+ and OH^- ions could be interchangeably used as charge-determining ions of the colloidal particles with no strong effect on the structure of the materials under study.

Note that the presence of large amount of OH-groups and physically adsorbed water on the surface of magnetic nanoparticles has been revealed by IR spectroscopy (bands at 3440, 1630, 823 and 1045 cm^{-1}) [8,24]. These results indicate that the prepared materials are highly hydrophilic to form stable aqueous suspensions or sols suitable for biomedical applications.

According to the TEM characterization, the morphology of all the compositions of the ferrites are similar. A typical TEM image of the nanoparticles (sample Zn-0.18) prepared by sol-gel method using inorganic precursors is given in Fig. 3. The oxide particles have a nearly spherical shape with a diameter ranging from 4 to 10 nm. The average grain size was estimated from the electron microscopy images to be ~6 nm, which corresponds well to the size estimated from the XRD patterns by the Scherrer Eqn (1). It is important to point out that the particle size distribution of the prepared materials is merely identical to the distribution estimated in Ref. [8] taking into account the difference in nature of the ions stabilizing the sols.

Mössbauer spectra of the obtained samples measured at room temperature and at 78 K are given in Fig. 4. For comparison, Fig. 4 (*a*, *g*) also shows the spectra of bulk Fe_3O_4 oxide prepared by reduction of α-Fe_2O_3 in 10% H_2 in Ar flow. At 298 K, the later spectrum consists of two Zeeman components with isomer shifts (ISs) of ~0.29 mm/s and ~0.67 mm/s,

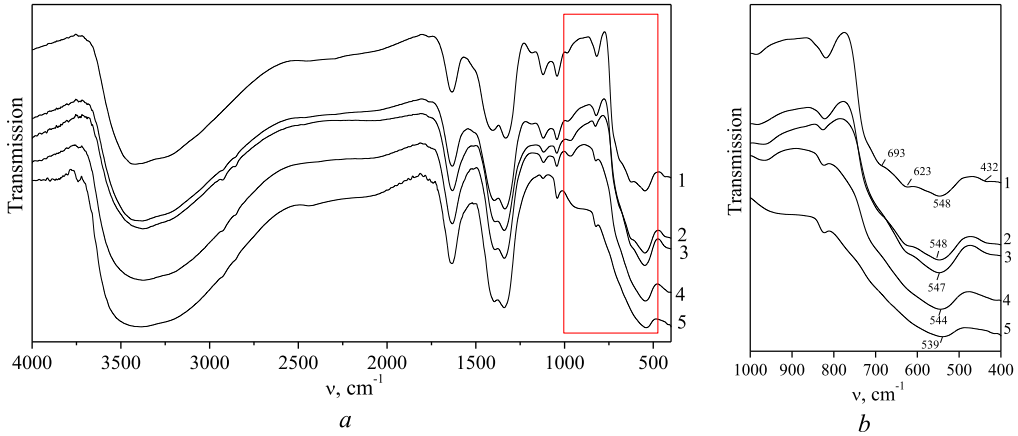

Fig. 2. Whole range (*a*) and scaled (*b*) IR spectra of magnetite and Zn-substituted ferrites:1– Zn-0; 2 – Zn-0.09; 3 – Zn-0.18; 4 – Zn-0.45; 5 – Zn-1.

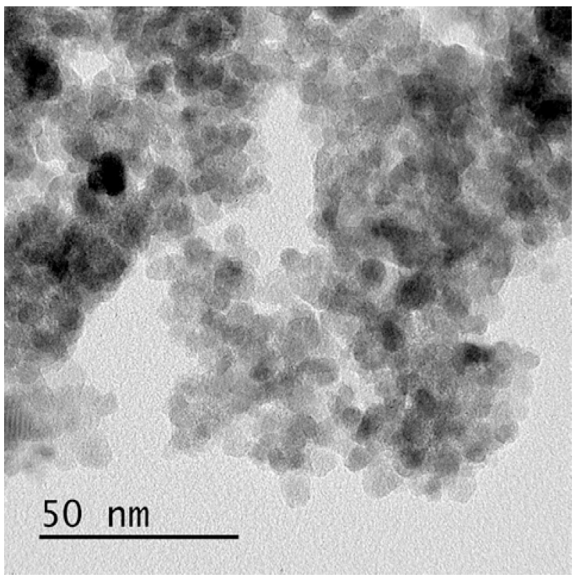

Fig. 3. TEM image of Zn-0.18 sample.

corresponding to Fe^{3+} in the tetrahedral sublattice and $Fe^{2.5+}$ mixed valence cations (because of $Fe^{2+} \leftrightarrow Fe^{3+}$ fast electron exchange) in the octahedral sublattice, respectively. The area ratio $I_{tet}(Fe^{3+})/I_{oct}(Fe^{2.5+})$ is close to the ideal value of 0.5. At 78 K, which is below the Verwey temperature (~120 K), Fe_3O_4 crystal structure changes from cubic to monoclinic [25]. The transformation is accompanied by the partial charge disproportionation in the octahedral sublattice of spinel structure that makes the Mössbauer spectrum complicated (Fig. 4g). The shape of the spectrum is asymmetrical and it is fitted with five Zeeman components, corresponding to Fe^{3+} cations in octahedral and tetrahedral sites, and Fe^{2+} cations in octahedral sites (Table 2) [25]. The spectral area ratio $I(Fe^{2+})/I(Fe^{3+})$ is close to the ideal 0.5.

The spectrum of Zn-0 unsubstituted sample recorded at 298 K is shown if Fig. 4b. Similar to the bulk Fe_3O_4, it also consists of two magnetically split subspectra corresponding to Fe^{3+} (IS ~ 0.3 mm/s) and $Fe^{2.5+}$ (IS ~ 0.6 mm/s) cations. The latter subspectrum is highly broadened and was fitted by a distribution of hyperfine magnetic fields, $P(H)$, using Hesse and Rubartsch approach [26], with IS ~ 0.6 mm/s within 41–48 T H_{hf} range. However, the area ratio $I(Fe^{3+})/I(Fe^{2.5+})$ of ~ 2.5 is significantly higher than that of ~ 0.5 for the bulk Fe_3O_4 (see Table 2). This confirms the supposition about a partial oxidation of Fe^{2+} cations made during the discussion of the XRD and IR spectroscopy results on possible γ-Fe_2O_3 formation. The low temperature (78 K) spectrum (Fig. 4h) has a complicated asymmetrical shape similar to that of bulk Fe_3O_4. Here again, the spectral contribution of Fe^{3+} cations is much higher as compared to the stoichiometric bulk Fe_3O_4, viz. experimental $I(Fe^{2+})/I(Fe^{3+})$ is ~ 0.18 vs. ideal 0.5. Since Fe_3O_4 and γ-Fe_2O_3 phases

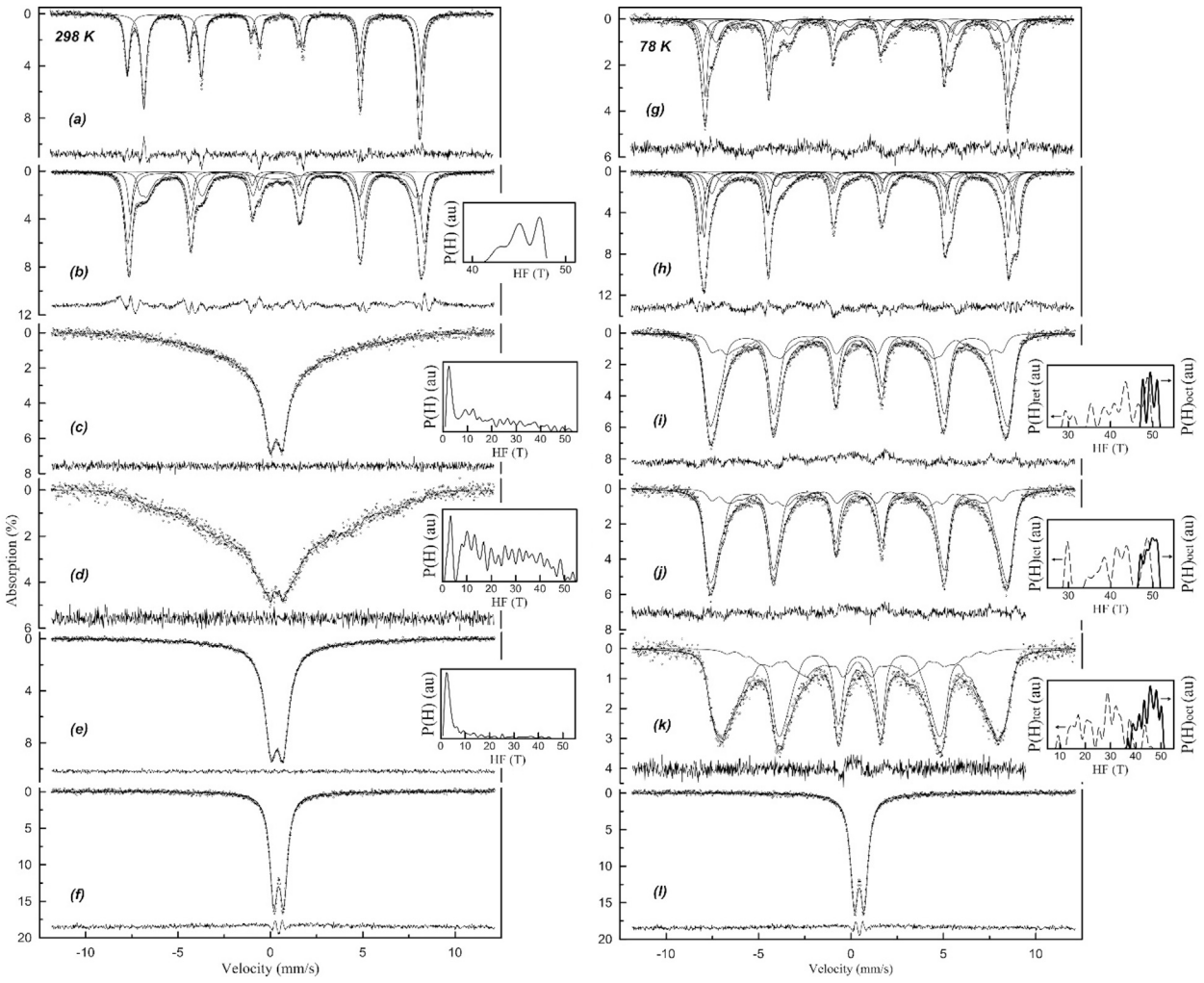

Fig. 4. ^{57}Fe Mössbauer spectra of the ferrites recorded at 298 K (*a–f*) and 78 K (*g–l*): (a, g) – bulk Fe_3O_4; (*b, h*) – sample Zn-0; (*c, i*) – sample Zn-0.09; (*d, j*) – Zn-0.18; (*e, k*) – sample Zn-0.45; (*f, l*) – sample Zn-1. The corresponding $P(H)$ distributions for tetrahedral and octahedral positions are given in the inlays.

Table 2
Parameters of ^{57}Fe Mössbauer spectra of the samples (IS – isomer shift, ΔE_Q – quadrupole splitting, H_{hf} – hyperfine magnetic field or range of field for $P(H_{hf})$ distributions, I – relative area, Γ – full width at half maximum of height).

Sample	T, K	Component	IS, mm/s ± 0.01	ΔE_Q, mm/s ± 0.01	H_{hf}, T ± 0.1	I, % ± 1	Γ, mm/s ± 0.01	Assignment
Fe_3O_4 bulk	300	Sb1	0.29	0.01	49.3	37	0.30	$Fe^{3+}_{(t)}$
		Sb2	0.66	0.01	46.1	63	0.32	$Fe^{2.5+}_{(o)}$
	78	Sb3	0.39	0.00	50.8	35	0.31	$Fe^{3+}_{(t)}$
		Sb4	0.53	0.00	52.9	21	0.42	$Fe^{3+}_{(o)}$
		Sb5	0.73	−0.11	50.7	11	0.37	$Fe^{3+}_{(o)}$
		Sb6	0.95	−0.62	48.8	24	0.69	$Fe^{2+}_{(o)}$
		Sb7	1.14	1.78	36.4	10	0.58	$Fe^{2+}_{(o)}$
Zn-0	300	S11	0.28	−0.01	48.5	18	0.30	$Fe^{3+}_{(t)}$ in Fe_3O_4
		Di11	0.59	0	<41–48>	28	–	$Fe^{2.5+}_{(o)}$ in Fe_3O_4
		S12	0.34	−0.02	49.7	47	0.46	Fe^{3+} in γ-Fe_2O_3
		D11	0.32	0.01	–	8	3.00	
	78	S13	0.35	0.00	50.9	26	0.32	$Fe^{3+}_{(t)}$
		S14	0.51	−0.02	53.1	31	0.40	$Fe^{3+}_{(o)}$
		S15	0.50	0.06	51.1	13	0.33	$Fe^{3+}_{(o)}$
		S16	0.49	−0.15	48.7	15	0.56	$Fe^{3+}_{(o)}$
		S17	1.03	−0.25	48.0	9	0.70	$Fe^{2+}_{(o)}$ in Fe_3O_4
		S18	1.33	1.46	35.6	6	0.76	$Fe^{2+}_{(o)}$ in Fe_3O_4
Zn-0.09	300	Di21	0.33	0	<1–50>	100	–	Fe^{3+}
	78	Di22	0.34	0	<27–50>	33	–	$Fe^{3+}_{(t)}$
		Di23	0.45	0	<47–52>	67	–	$Fe^{3+}_{(o)}$
Zn-0.18	300	Di31	0.35	0	<1–51>	100	–	Fe^{3+}
	78	Di32	0.34	0	<27–50>	26	–	$Fe^{3+}_{(t)}$
		Di33	0.45	0	<46–52>	74	–	$Fe^{3+}_{(o)}$
Zn-0.45	300	Di41	0.35	0	<0–40>	100	–	Fe^{3+}
	78	Di42	0.34	0	<10–45>	25	–	$Fe^{3+}_{(t)}$
		Di43	0.45	0	<35–52>	75	–	$Fe^{3+}_{(o)}$
Zn-1	300	D51	0.34	0.53	–	100	0.43	$Fe^{3+}_{(o)}$
	78	D52	0.45	0.54	–	100	0.51	$Fe^{3+}_{(o)}$

have the same spinel crystal structure, the hyperfine parameters of Fe^{3+} cations are very similar in both cases. Considering the broadening and overlapping of the components, the exact phase assignments for Fe^{3+} cations becomes ambiguous.

The Mössbauer spectra of the Zn-substituted samples (Zn-0.09, Zn-0.18 and Zn-0.45) are shown in Fig. 4 (*c–e*, *i–k*). The symmetrical shapes of the spectra at both 298 K and 78 K temperatures are significantly different from that for the unsubstituted Zn-0 sample, suggesting that all the Fe cations are in the same oxidation state. At 298 K, the broad magnetic relaxation type spectra were described by $P(H)$ distributions with IS ~ 0.35 mm/s, corresponding to exclusively Fe^{3+} cations (Fig. 4, Table 2). The spectra at 78 K consist of broaden magnetically split components, but retain their symmetrical shape. The best fittings were obtained with a superposition of two $P(H)$ distributions with IS ~ 0.45 and ~ 0.34 mm/s, assigned to Fe^{3+} cations in octahedral and tetrahedral positions in the spinel lattice (see Table 2). The spectra obtained for the Zn-substituted samples differ from those reported for the Zn-substituted Fe_3O_4, but they are similar to the spectra of pure and doped γ-Fe_2O_3 [27,28]. Therefore, according to the Mössbauer study, the substitution of iron with zinc led to a complete oxidation of Fe^{2+} ions to Fe^{3+} state with the formation of cation vacancy bearing spinel-type solid solutions ($Zn_xFe_{3-x-y}\square_yO_4$) from γ-$Fe_2O_3$–$ZnFe_2O_4$ quasi-binary system.

According to the data given in Table 2, semi-quantitatively, the contributions of tetrahedral Fe^{3+} decrease with the growth of zinc content, since Zn^{2+} ions have a tendency to occupy tetrahedral sites of spinel lattice. The spectra of Zn-1 sample ($ZnFe_2O_4$) in Fig. 4 (*f*, *l*) represent paramagnetic single doublets for both 298 K and 78 K, similarly to bulk $ZnFe_2O_4$ [29]. The hyperfine parameters of the doublets are typical of Fe^{3+} in octahedral oxygen coordination, which is consistent with the normal spinel crystal structure of $ZnFe_2O_4$.

It is worth noting that $Zn_xFe_{3-x-y}\square_yO_4$oxide materials that do not contain Fe^{2+} cations are not oxidized under ambient conditions. In case of *in vivo* applications, they are potentially more stable than analogous magnetite-based materials. The depth of Fe_3O_4 oxidation to γ-Fe_2O_3 rises with decreasing grain size. The oxidation effect is the most pronounced in case of nanoparticles with diameters less than 10 nm.

Based on the results of Mössbauer spectroscopy, providing actual Fe^{3+} contents in the samples, and the XRD data, evidencing the presence of main spinel phase and the absence of others phases, actual compositions of the studied samples were calculated. The calculations were made taking into account (i) experimentally obtained Fe^{3+} contents in the samples, i.e. Fe^{2+} oxidation, and (ii) cation vacancy formation in spinel structure for charge compensation due to heterovalent substitution of Fe^{2+} cations with Fe^{3+} ones (again because of oxidation) according to the scheme: $3Fe^{2+} = 2Fe^{3+} + \square_{Fe}$. The calculated actual compositions of the Zn-doped samples together with their magnetic properties are listed in Table 3.

The magnetic properties of the prepared nanomaterials were estimated from the specific magnetization curves as a function of magnetic field strength recorded at low (5 K) and room temperatures (Fig. 5). The magnetization and coercivity values measured for the powdered samples were correlated with their structure in Table 3. The main regularities of the magnetic behavior of the powders are discussed in Ref. [8].

At 5 K, there is a clear effect of zinc content on the magnetic properties of the Zn-substituted magnetite. The concentration of Fe^{3+} ions in tetrahedral sites of the spinel-type lattice measured at 78 K decreases

Table 3
Composition, maximum magnetization and coercivity of the $Zn_xFe_{3-x-y}\square_yO_4$ nanosized particles as a function of Zn content.

x	0	0.09	0.18	0.45	1
Refined composition	$Fe_{2.79}\square_{0.21}O_4$	$Zn_{0.08}Fe_{2.61}\square_{0.31}O_4$	$Zn_{0.16}Fe_{2.56}\square_{0.28}O_4$	$Zn_{0.42}Fe_{2.39}\square_{0.19}O_4$	$ZnFe_2O_4$
I_{max} (5 K), emu/g	62	64	80	86	45
I_{max} (300 K), emu/g	49	51	59	46	9
H_c (5 K), Oe	500	320	270	240	200

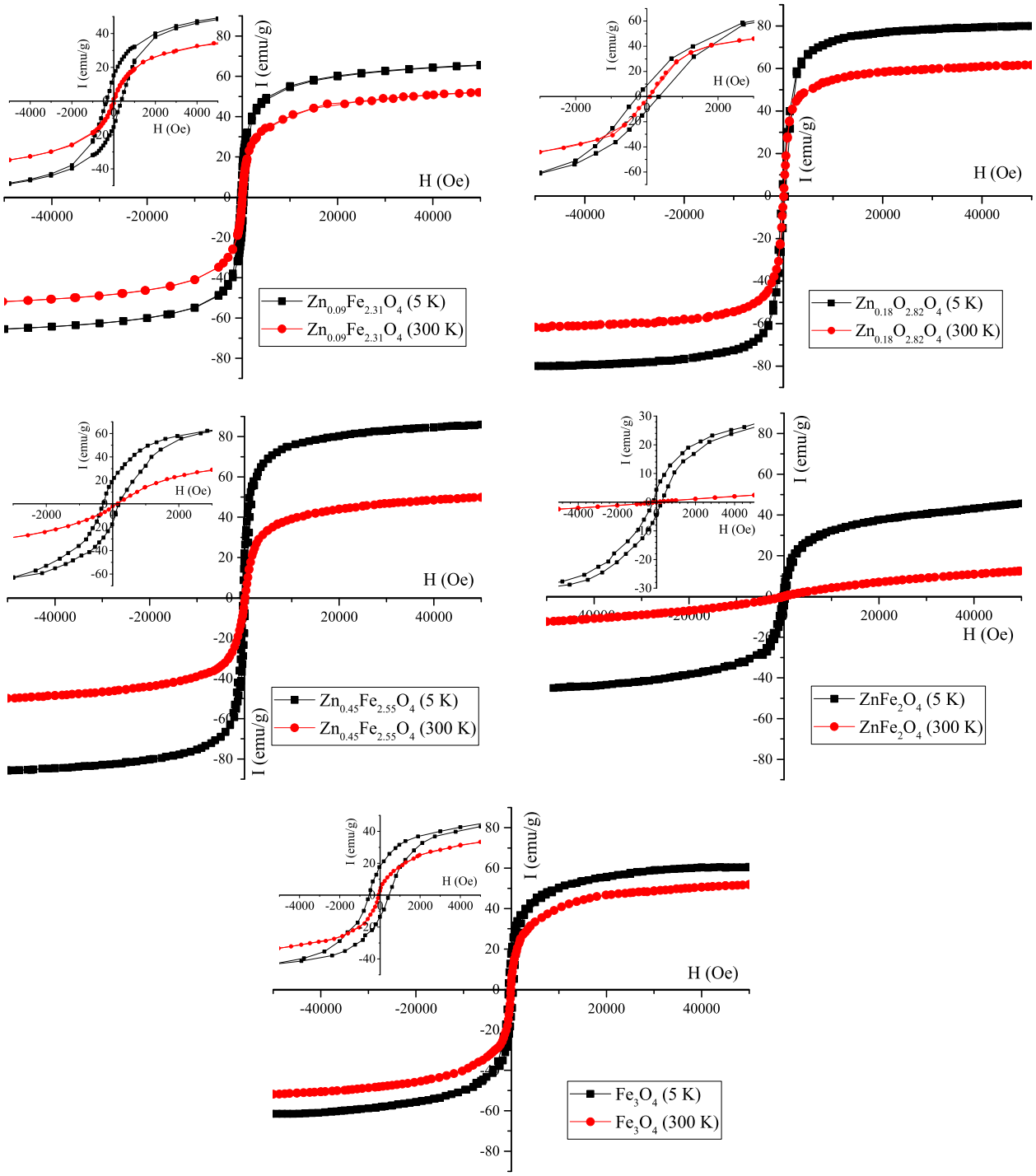

Fig. 5. Specific magnetization curves of pure magnetite and Zn-substituted ferrites at 300 and 5 K; the hysteresis loops recorded at low field are on insert graphs.

with increasing amount of Zn^{2+} ions up to $x = 0.45$ (see Table 2, 78 K), which causes the magnetization growth [8,30]. Note that at 5 K, the difference between Zn^{2+} contents in tetrahedral sites of the samples with x = 0.18 and 0.45 should be more pronounced. Thus, the maximum magnetization is expected for $Zn_{0.42}Fe_{2.39}\square_{0.19}O_4$ composition with $x = 0.45$, which was confirmed experimentally (the measured value is 86 emu/g at 5 K).

At room temperature, a maximum magnetization value ($I = 59$ emu/g) was demonstrated by $Zn_{0.16}Fe_{2.56}\square_{0.28}O_4$ sample ($x = 0.18$). This behavior could be attributed to the formation of the magnetically dead layer at the surface of the magnetic nanoparticle [31,32]. Due to a high surface to volume ratio of the nanoparticles, the order of the surface magnetic moments plays an important role in determining the magnetic properties of a whole ferrite particle. The dead layer is formed due to the discontinuity of magnetic interaction of the surface. This causes the magnetization of nanoparticles to be lower than the bulk ones [32]. Doping magnetite with Zn was found to lead to the growth of the dead layer thickness. It is claimed, that the sample with $x = 0.2$ has the smallest dead layer thickness at room temperature [31]. The indicated substitution value is close to $Zn_{0.16}Fe_{2.56}\square_{0.28}O_4$ sample ($x = 0.18$) with the highest magnetization at 300 K. At low temperature, the surface of the particles is believed to become less disordered, and has a minor effect on the magnetization. Thus, the ions redistribution plays the main role in determining the magnetic properties of Zn-substituted magnetite at 5 K.

4. Conclusions

Sol-gel method based on using inorganic metal salts has been successfully used to prepare superparamagnetic nanoparticles of $Zn_xFe_{3-x}O_4$ solid solutions with different zinc content and a narrow size distribution. Doping of magnetite with zinc was found to promote a complete oxidation of Fe^{2+} ions with oxygen to form spinel-type solid solutions containing cation vacancies ($Zn_xFe_{3-x-y}\square_yO_4$). The absence of Fe^{2+} state and an increased colloidal stability of the aqueous dispersions of the ferrites may facilitate the metabolism of the nanoparticles in living organisms. The magnetic properties of the synthesized ferrites show non-linear dependence from the zinc content. At 5 K, $Zn_{0.42}Fe_{2.39}\square_{0.19}O_4$ sample with an intermediate Zn content (x = 0.45) has the highest magnetization (I = 86 emu/g) due to the maximum concentration of Fe^{3+} ions in the tetrahedral sites of spinel lattice. At room temperature, a maximum magnetization value (I = 59 emu/g) was achieved for $Zn_{0.16}Fe_{2.56}\square_{0.28}O_4$ sample with x = 0.18, which is possibly related to the smallest thickness of the magnetically disordered surface layer at the given degree of Zn substitution. The small grain size and relatively high magnetization values of the prepared Zn-substituted magnetites make them promising materials for biomedical use, especially for contrast-enhanced magnetic resonance imaging.

References

[1] B. Issa, I.M. Obaidat, B.A. Albiss, et al., Magnetic nanoparticles: surface effects and properties related to biomedicine applications, Int. J. Mol. Sci. 14 (2013) 21266–21305.
[2] M. Colombo, S. Carregal-Romero, M.F. Casula, et al., Biological applications of magnetic nanoparticles, Chem. Soc. Rev. 41 (2012) 4306–4334.
[3] Q.A. Pankhurst, J. Connolly, S.K. Jones, et al., Applications of magnetic nanoparticles in biomedicine, J. Phys. D. Appl. Phys. 36 (2003) R167–R181.
[4] L.H. Reddy, J.L. Arias, J. Nicolas, et al., Magnetic nanoparticles: design and characterization, toxicity and biocompatibility, pharmaceutical and biomedical applications, Chem. Rev. 112 (2012) 5818–5878.
[5] P. Tartaj, M.P. Morales, S. Veintemillas-Verdaguer, et al., The preparation of magnetic nanoparticles for biomedical applications in biomedicine, J. Phys. D. Appl. Phys. 36 (2003) R182–R197.
[6] W. Wu, Q. He, C. Jiang, Magnetic iron oxide nanoparticles: synthesis and surface functionalization strategies, Nanoscale Res. Lett. 3 (2008) 397–415.
[7] A.K. Gupta, M. Gupta, Synthesis and surface engineering of iron oxide nanoparticles for biomedical applications, Biomaterials 26 (2005) 3995–4021.
[8] E. Petrova, D. Kotsikau, V. Pankov, Structural characterization and magnetic properties of sol-gel derived $Zn_xFe_{3-x}O_4$ nanoparticles, J. Magn. Magn. Mater 378 (2015) 429–435.
[9] A.G. Kolhatkar, A.C. Jamison, D. Litvinov, et al., Tuning the Magnetic properties of nanoparticles, Int. J. Mol. Sci. 14 (2013) 15977–16009.
[10] H.H. Hamdeh, J.C. Ho, S.A. Oliver, et al., Magnetic properties of partially-inverted zinc ferrite aerogel powders, J. Appl. Phys. 81 (1997) 1851–1857.
[11] J.F. Hochepied, P. Bonville, M.P. Pileni, Nonstoichiometric zinc ferrite nanocrystals: synthesis and unusual magnetic properties, J. Phys. Chem. B 104 (2000) 905–912.
[12] J. Wan, X. Jiang, H. Li, et al., Facile synthesis of zink ferrite nanoparticles as non-lanthanide T_1 MRI contrast agents, J. Mater. Chem. 22 (2012) 13500–13505.
[13] W. Schiessl, W. Potzel, H. Karzel, et al., Magnetic properties of the $ZnFe_2O_4$ spinel, Phys. Rev. B 53 (1996) 9143–9152.
[14] B.D. Cullity, Introduction to Magnetic Materials, first ed., Addison Wesley, New York, 1972.
[15] D. Venkateshvaran, M. Althammer, A. Nielsen, et al., Epitaxial $Zn_xFe_{3-x}O_4$ thin films: a spintronic material with tunable electrical and magnetic properties, Phys. Rev. B 79 (2009) 134405.
[16] M. Ivanovskaya, D. Kotsikau, A. Taurino, et al., Structural distinctions of Fe_2O_3-In_2O_3 composites obtained by various sol-gel procedures, and their gas-sensing features, Sens. Actuators B 124 (2007) 133–142.
[17] A. Adakimchik, I. Azarko, M. Ivanovskaya, et al., Transport and magnetic resonance characteristics of SiO_2–γ-Fe_2O_3 composites obtained by sol-gel method, Przeglad elektrotechniczny 84 (2008) 212–213.
[18] E. Tombacz, A. Majzik, Zs Horvat, et al., Magnetite in aqueous medium: coatings its surface and surface coated with, Rom. Rep. Phys. 58 (2006) 281–286.
[19] B. Gillot, R.M. Benloucif, A. Rousset, A study of infrared absorption in the oxidation of zinc-substituted magnetites to defect phase γ and hematite, J. Solid State Chem. 39 (1981) 329–336.
[20] E. Nazarenko, J.E. Lorenzo, Y. Joly, et al., Resonant X-ray diffraction studies on the charge ordering in magnetite, Phys. Rev. Lett. 97 (2006), 089902.
[21] A.C.S. Costa, I.G. Souza, M.A. Batista, et al., Structural, magnetic and hyperfine characterization of zinc-substituted magnetites, Hyperfine Interact. 175 (2007) 103–111.
[22] W. Kim, C.-Y. Suh, S.-W. Cho, et al., A new method for the identification and quantification of magnetite-magnemite mixture using conventional X-ray diffraction technique, Talanta 94 (2012) 348–352.
[23] J. Murbe, A. Rechtenbach, J. Topfer, Synthesis and physical characterization of magnetite nanoparticles for biomedical applications, Mater. Chem. Phys. 110 (2008) 426–433.
[24] F.-Y. Cheng, C.-H. Su, Y.-S. Yang, et al., Characterization of aqueous dispersions of Fe_3O_4 nanoparticles and their biomedical applications, Biomaterials 26 (2005) 729–738.
[25] A.C. Doriguetto, N.G. Fernandes, A.I.C. Persiano, E.N. Filho, J.M. Grenèche, J.D. Fabris, Characterization of a natural magnetite, Phys. Chem. Minerals 30 (2003) 249–255.
[26] J. Hesse, A. Rubartsch, Model independent evaluation of overlapped Mossbauer spectra, J. Phys. E Sci. Instrum. 7 (1974) 526.
[27] H. Mehner, H.J. Koppe, W. Mörke, Mössbauer investigations of γ-Fe2O3 particles, Hyperfine Interact. 54 (1990) 609–612.
[28] P.M. Zélis, G.A. Pasquevich, S.J. Stewart, M.B.F.v. Raap, J. Aphesteguy, I.J. Bruvera, C. Laborde, B. Pianciola, S. Jacobo, F.H. Sánchez, Structural and magnetic study of zinc-doped magnetite nanoparticles and ferrofluids for hyperthermia applications, J. Phys. D Appl. Phys. 46 (2013), 125006.
[29] V. Šepelák, S. Wißmann, K.D. Becker, A temperature-dependent Mössbauer study of mechanically activated and non-activated zinc ferrite, J. Mater. Sci. 33 (1998) 2845–2850.
[30] J.B. Goodenough, Magnetism and the Chemical Bond, Interscience Monographs on Chemistry, Inorganic Chemistry Section vol. I, Interscience-Wiley, New York, 1963, p. 121.
[31] H.M. El-Sayed, I.A. Ali, A. Azzam, A.A. Sattar, Influence of the magnetic dead layer thickness of Mg-Zn ferrites nanoparticle on their magnetic properties, J. Magn. Magn. Mater. 424 (2017) 226–232.
[32] T. Maehara, K. Konishi, T. Kamimori, et al., Selection of ferrite powder for thermal coagulation therapy with alternating magnetic field, J. Mater. Sci. 40 (2005) 135.